

An Analytical Study on Offset H-shaped Steel Beams to Square Concrete Filled Steel Tubular Column Connection Panels with Exterior Diaphragms

Mou, Ben

Department of Architecture, Graduate School of Human-Environment Studies, Kyushu University :
Doctoral Program

Matsuo, Shintaro

Department of Architecture and Urban Design, Faculty of Human-Environment Studies, Kyushu
University : Associate Professor

<https://doi.org/10.15017/1785658>

出版情報 : 都市・建築学研究. 28, pp.79-94, 2015-07-15. Faculty of Human-Environment Studies,
Kyushu University

バージョン :

権利関係 :



An Analytical Study on Offset H-shaped Steel Beams to Square Concrete Filled Steel Tubular Column Connection Panels with Exterior Diaphragms

段差を有する外ダイアフラム形式コンクリート充填角形鋼管 柱梁接合部パネルに関する解析的研究

Ben MOU* and Shintaro MATSUO**

牟 犇, 松尾真太郎

This paper presents an analytical study on offset H-shaped steel beam to square concrete filled steel tubular column connection panels with exterior diaphragms. This research focuses on the full plastic strength and collapse mechanisms of the offset beam-to-CFT column connection panels, and investigates the influence of difference in beam depth and width to thickness ratio on the elasto-plastic behaviors of the offset beam-to-CFT column connection panels. The feasibility of analytical models generated by MSC. Marc 2012 is verified by a set of experimental results presented in the companion paper. Parameters used in this analytical study includes: differences in beam depths, width to thickness ratio and loading directions. FEM results suggest that the assumed collapse mechanisms can predict the failure modes of FEM models reasonably. Owing to overlooking confined effect by steel tubes on concrete panels, the proposed formulae underestimated the full plastic shear strength of the offset panels. On the basis of experimental and analytical results, an enhancement coefficient formula is proposed, which is derived from regression analysis taking the effect of width to thickness ratio of steel tubes and beam depth ratio into consideration.

Keywords: *Offset beam-to-column connection panel, Exterior diaphragm, Concrete filled steel tube, Collapse mechanism, Full plastic strength, Finite element method analysis*
段違いパネル、外ダイアフラム、コンクリート充填鋼管、崩壊機構、全塑性耐力、有限要素法解析

1. Introduction

Concrete filled steel tubular (CFT) structures have been gradually adopted in mid- and high-rise buildings in recent years. Recommendations for design and construction of concrete filled steel tubular structures have been published ¹⁾.

With the development of technology and society, in practical structural design, steel or CFT structures must not only meet the needs of structural performance but also satisfy the demands of lower weight, securing the space for installing the equipment and so on. Connections, in which the beams on either side of the columns have a different depth, are often adopted in order to meet requirements of the above. This type of connection panel is called offset panel. With regard to the offset beam-to-CFT column connections with exterior diaphragms shown in Fig. 1, there is not the established design method in the current design guidelines. Therefore, in order to respond the demands of the above, the design method of the offset panel has to be developed as soon as possible. In

the companion paper ²⁾, an experimental study on offset H-shaped steel beams to square concrete filled steel tubular column connection with exterior diaphragms was presented. However, owing to the confined effect on concrete, the present proposed formulae underestimated the shear strength of the offset panel. Therefore, an analytical approach is essential in order to continue further study on the validity of the proposed formulae.

Researches on the FEM analysis of beam-to-CFT column connections have been nearly developed. Aolstaz and Schneider ³⁾ used two different approaches to model the interface between the steel tube and concrete. The first one added the gap element between the steel part and concrete part. However, there are convergence problems in many cases when using this element. The second one is that the interface was modelled using a thin layer of 20-node brick elements with very low strength and stiffness properties. There was almost no difference between the connection behaviour observed for the two interface models. Chiew et al.⁴⁾ simulated the behavior of I shaped steel beam to CFT column connections by using MSC. Marc 2012 ⁵⁾. According to the

* 空間システム専攻 博士後期課程

** 都市・建築学部門

experimental and analytical results, appropriate empirical formulae were proposed.

This paper presents analytical investigation on the offset beam-to-CFT column connection panels with exterior diaphragms. Fourteen finite element models are generated. The main objectives consist of some aspects. The first objective is to verify the feasibility of FEM models by comparing with fundamental data obtained by the loading tests in the companion paper ²⁾. The second one is to clarify collapse mechanisms of offset beam-to-CFT column connection panels with exterior diaphragms. Furthermore, based on the assumed collapse mechanisms, calculation formulae of the full plastic shear strength of the offset panels are proposed. On the basis of experimental and analytical results, the last objective is to propose an enhancement coefficient formula, which is derived from regression analysis taking the effect of width to thickness ratio of steel tubes and beam depth ratio into consideration.

2. Simulation of the experimental results

Four specimens in the previous experimental study ²⁾ have been conducted. The analytical models are validated by comparing FEM analysis results with the experimental data.

2.1 Outline of the tests ²⁾

Summaries of specimens are listed in Table 1. A typical cruciform specimen and the details of divided exterior diaphragm are shown in Figs. 2 (a) and (b), respectively. The main experimental parameters were difference in beam depth ($\Delta d_b=0\text{mm}, 75\text{mm}, 150\text{mm}$) and loading types (cyclic loading and monotonic loading). As for the test device, a pin and vertically-roller support was connected with a steel frame at the top of the square CFT column. And a pin support was at the end of column bottom. The length between the pin and the pin roller was 1800mm, and the length between the two loading points was 2700mm. Two hydraulic jacks of 500kN capacity were used to apply the loadings to the beam ends in the vertical direction. In the positive direction, the beam 1 end was pulled upward, while the beam 2 end was pushed downward. In the negative direction, the loadings on the beam ends were reversed. Out-of-plane movement restraint devices were designed to prevent the unexpected instability and lateral torsional buckling of the specimens.

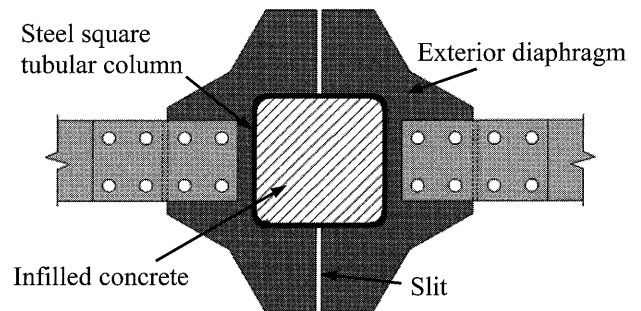
2.2 Analytical model of FEM analysis

MSC. Marc 2012 ⁵⁾ is selected for the current analysis. The analytical model is composed of several parts such as beams at both sides of connection, square steel tubular column, exterior diaphragms, fillet weld metal, two rigid plates and filled concrete. They are modelled as half models using boundary conditions for the symmetry. A schematic of the

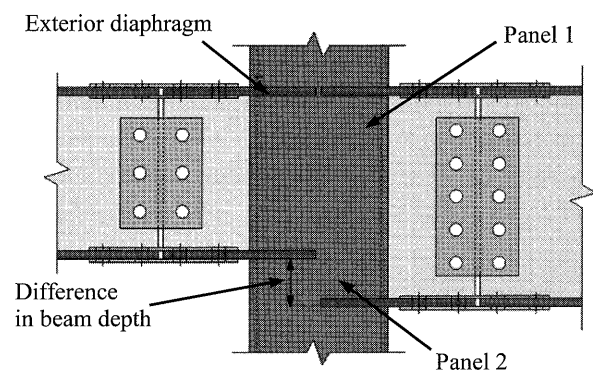
FEM model for a typical subassembly is shown in Fig. 3. Element type7 (8-node, isoparametric, arbitrary hexahedral solid element) in Marc 2012 is used to mesh the offset beam-to-CFT column connection models.

Material properties for steel are listed in Table 2. Steel is modelled by elasto-plastic material. It is assumed that all steel components behave the same in compression as in tension. Material properties of steel parts are defined as nonlinear isotropic model. True stress-logarithmic plastic strain curves from coupon material tests are used to specify the plastic parts of elasto-plastic characteristics. Yield criterion is based on the von Mises yield criterion, and kinematic hardening rule is adopted in the analysis. True stress-logarithmic plastic strain curves for exterior diaphragms, beam flange, fillet weld metal, beam web and steel tubular column are shown in Fig. 4 (a).

Material properties for concrete are listed in Table 3. Poisson's ratio of concrete is assumed as 0.2 and Young's modulus is on the basis of cylinder compression test. Stress-strain relationship of compression envelope consists of a nonlinear increasing branch up to the ultimate strength and a descending branch. The increasing branch is obtained by results of the cylinder compression test. The descending branch is described by linear. The uniaxial stress-strain



(a) Divided exterior diaphragm ⁹⁾



(b) Offset beam-to-CFT column connection

Fig. 1 Offset H-shaped steel beam to square CFT column connection with exterior diaphragms

Table 1 Details of specimens

No.	Steel column (BCR295)	Beam 1 (SN490B)	Beam 2 (SN490B)	Δd_b [mm]	Loading type
1	□- 200×200×9	BH- 300×120×6×12	BH-300×120×6×12	0	Cyclic
2			BH-225×120×6×12	75	
3			BH-150×120×6×12	150	Monotonic
4					

BCR295 is the material approved by the ministry of land, infrastructure, and transport in Japan. SN490B is the material specified in Japanese industrial standard

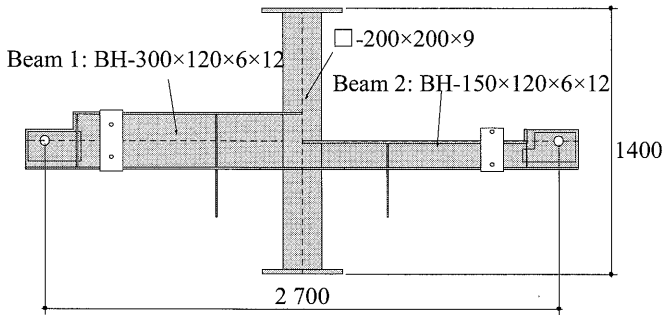


Fig. 2 (a) Specimen (No.3 and No.4)

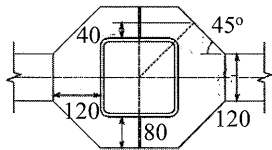


Fig. 2 (b) Details of exterior diaphragm

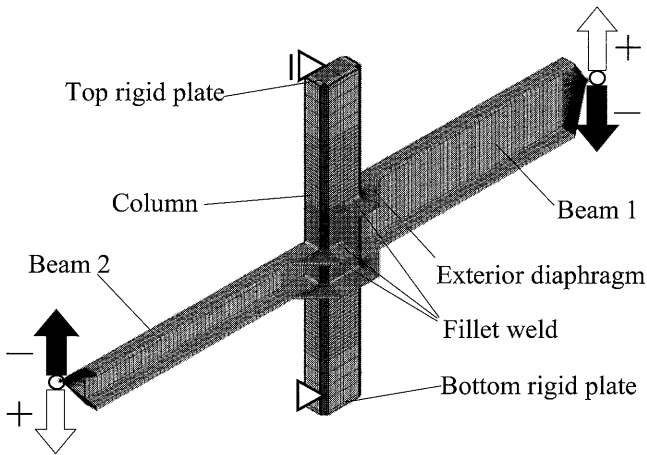


Fig. 3 Finite element model for the offset beam-to-CFT column connection

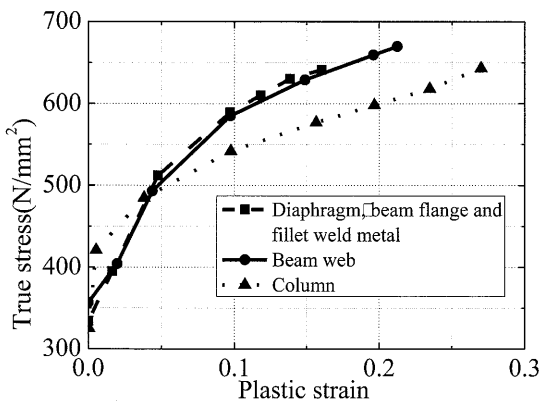


Fig. 4 (a) True stress-plastic strain curves for steel

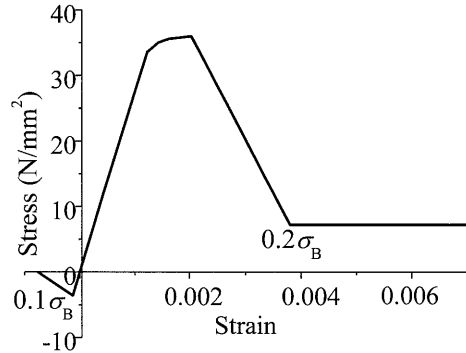


Fig. 4 (b) Stress-strain relation for concrete

Table 2 Material properties for steel

Part	Thickness [mm]	Young's modulus [N/mm ²]	Yield stress [N/mm ²]
Beam web	6.2	201,700	399
Beam flange	11.9	207,240	351
Exterior diaphragm			
Fillet weld metal	9.0	192,300	371
Square column			

Table 3 Material properties for concrete

No.	Young's modulus [N/mm ²]	Compressive strength (σ_B) [N/mm ²]
1	27,500	36.0
2	29,300	36.5
3	28,200	37.9
4	30,000	36.8

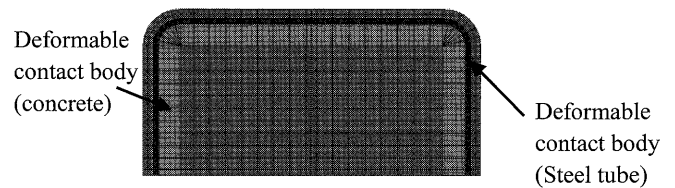


Fig. 5 Contact body defined by possible contacting elements

behavior used for concrete material model is shown in Fig. 4 (b)^{3,4}. Cracking is considered to be an important issue, and therefore accommodating these cracks dominates the development of this material model. Cracking model is chosen as damage effects. Critical cracking stress, tension softening modulus and shear retention factor are assumed to

be one to tenth of compressive stress, one to fifth of Young's modulus and 0.5, respectively ⁵⁾.

2.3 Contact description

Contact problems between concrete and steel tube are solved by using the direct constraint method in Marc 2012. The outermost layer of the concrete elements and the innermost layer of the steel tube elements are defined as deformable contact bodies that may contact with each other. These two deformable contact bodies are allowed to separate from each other while penetration is not allowed. It is more efficient to choose subset of the physical bodies which are likely to be involved in contact (see Fig. 5) since less checking for contact is required at each solution step. In three dimensional deformable contact, contact segments are the element faces on the surface of the contact bodies. The default tolerance in Marc 2012 is one twentieth of the edge length of the smallest element. In this research, the default tolerance is selected.

2.4 Procedure of FEM analysis

In order to simulate the experimental supporting conditions at the top and bottom ends of a column, rigid plates are connected to both ends, and a column is supported through the rigid plates. The supporting condition at the column top is a pin and vertically-roller support, and that at the column bottom is a pin support. The cross sections of beams at the both free ends remain planes, respectively, by the constraining option of nodal displacements in the cross sections. The vertical loading applied on the right and left sides of the specimen are controlled with the opposite of the direction in order to simulate the story drift angle caused by lateral loading. The story drift angle (R) is defined as the ratio of the vertical displacement between the ends of beam to the distance between the pins. The vertical loads at the free ends of beams are applied in a way that the increment of displacements is prescribed in the vertical direction up to 81mm ($R=0.06$ rad).

Arc length procedure is adopted in FEM analysis and Newton-Raphson incremental iteration method is used in the solution. The vertical loads are applied on all analytical

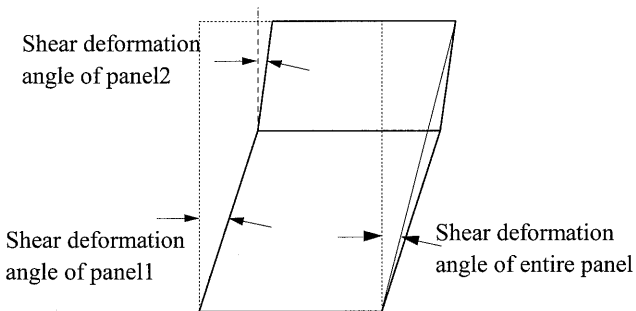
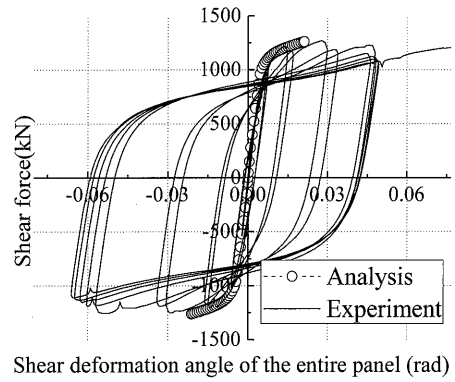
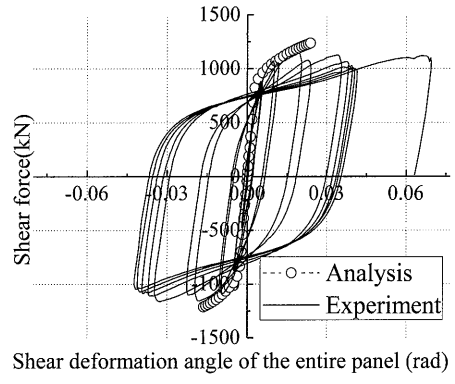


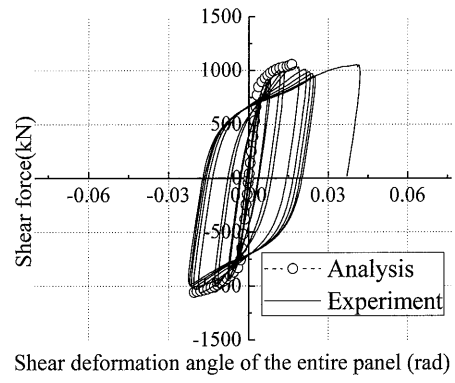
Fig. 6 Definition of shear deformation angle



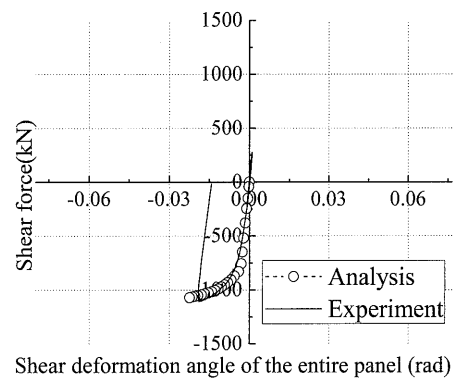
(a) No.1 ($\Delta d_b=0$, cyclic loading)



(b) No.2 ($\Delta d_b=75$, cyclic loading)

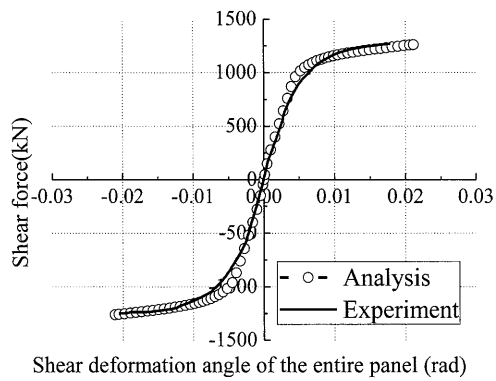


(c) No.3 ($\Delta d_b=150$, cyclic loading)

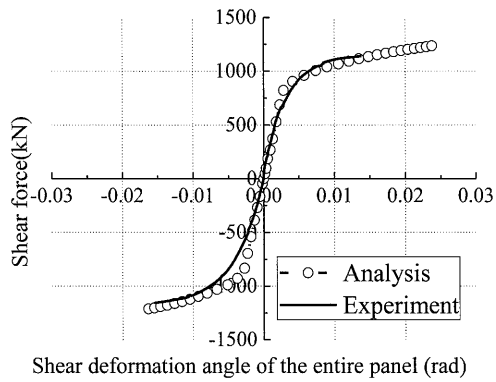


(d) No.4 ($\Delta d_b=150$, monotonic loading)

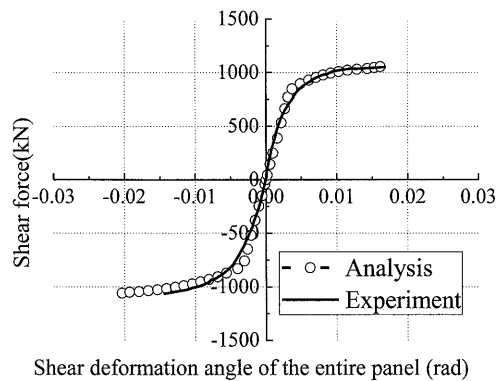
Fig. 7 Relations between shear force and shear deformation angle of the entire panel



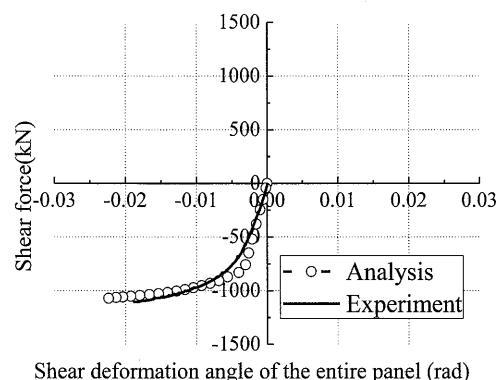
(a) No.1 ($\Delta d_b=0$, cyclic loading)



(b) No.2 ($\Delta d_b=75$, cyclic loading)



(c) No.3 ($\Delta d_b=150$, cyclic loading)



(d) No.4 ($\Delta d_b=150$, monotonic loading)

Fig. 8 Comparisons of shear strain of panel1 and panel2

Table 4 Experimental and analytical results

No.	Full plastic strength (kN)				pQ_{pFEM}/pQ_{pe}	
	pQ_{pFEM} (positive)	pQ_{pFEM} (negative)	pQ_{pe} (positive)	pQ_{pe} (negative)	(positive)	(negative)
1	1,094	1,094	1,119	1,087	0.99	1.02
2	1,004	1,055	1,033	997	0.97	1.04
3	897	914	918	914	0.93	0.97
4		910		859		1.00

Where, pQ_{pFEM} : 0.35% offset strength by FEM analysis, pQ_{pe} : 0.35% offset strength by tests

models of FEM analysis until the load points reach target displacement.

2.5 Discussion of the FEM analysis results

The definition of shear deformation angle of panel 1, panel 2 and entire panel are shown in Fig. 6. And relations between shear force and shear deformation angle of the entire panel, which are obtained from the FEM analysis, are compared to experimental results in Fig. 7. These figures show very good agreement between the analytical and experimental results. Whether the loading type is monotonic loading or cyclic loading, there are few differences between the FEM results and experimental results. Comparisons between the experimental results and FEM results for specimens are listed in Table 4. Experimental full plastic strength (pQ_{pe}) and analytical full plastic strength (pQ_{pFEM}) are obtained by 0.35% offset strength⁶⁾. Analytical full plastic strength is 93% to 104% of the experimental results. The full plastic strengths obtained by analytical results fluctuate around those obtained by the experimental results.

Relations between shear force and shear deformation of the entire panel obtained from FEM analysis are compared to skeleton curves measured by displacement transducers in Fig. 8. It can be seen that two curves agree well from the elastic stage to plastic stage. The analytical models accurately simulate the experimental results.

A generally good agreement is achieved between the deformation of entire panel predicted by using the FEM models and that observed in the test. Some typical comparisons between the experimental and predicted failure modes are shown in Fig. 9. For No.2 and No.3, it is found that the shear deformation of connection panel concentrates on panel 1. In addition, the deformations of panel 2 and beam web are very limited. In FEM results, owing to the differences in beam depth, visible yield areas are observed on the steel tubular flange connected with the exterior diaphragms.

Failures of the filled concrete at the panel in the experimental and FEM results are observed by removing part of the skin plate of the tube around the connection. Fig. 10 shows the stress distribution of the exposed concrete in No.2 and No.3. In the FEM results, obvious diagonal yield area indicates that the filled concrete forms arch mechanisms and

bears shear force transmitted by the exterior diaphragms. While, the heights of diagonal yield areas are different under the different loading directions. Owing to the specimens under the positive loading, arch mechanism of concrete forms through the entire panel. While, due to the specimens under the negative loading, only the panel 1 forms arch mechanism. The filled concrete of panel 2 has little contributions to resist shear force. Therefore, the concrete panels form different height compression arches in the different direction loadings. Behavior of the concrete panel in No.3 is similar to that in No.2. Owing to the difference in beam depth, the height of the diagonal yield area in the negative loading in No.3 is smaller than that in No.2.

2.6 Influence of parameters on the shear strength of entire panel

In order to determine the effect of width to thickness ratio and difference in beam depth on the shear strength of entire panel, additional FEM analysis is performed. Ten models are established. The main analytical parameters are difference in beam depth ($\Delta d_b = 0 \text{ mm}, 100 \text{ mm}, 200 \text{ mm}, 300 \text{ mm}$) and width to thickness ratio ($D/t = 21, 25, 33, 44$). As for low or middle rise residential buildings, the storey height ranges from 2.7 m to 3.3 m. And the range of span is centered on 4 m to 6 m⁷⁾. Dimensions of cruciform frame model in

horizontal and vertical directions are 5,000 mm and 2,800 mm, respectively, which are measured between the loading points and pins. Summary of the analysis models is shown in Table 5.

Steel is modelled as elastic-plastic material. Young's modulus and Poisson's ratio of the steel are assumed as 205,000 N/mm² and 0.3, respectively. Material properties for the steel tube are modelled after BCR295 with fully nonlinear isotropic characteristics. And yield strength is 295 N/mm². Material properties for the beam and exterior diaphragm are modelled after SN490B and their yield strength is 325 N/mm². Stress-strain relationship of the steel beam and steel tube are shown in Figs. 11 (a) and (b). Numerical analyses account for material non-linearities through classical metal plasticity theory based on the von Mises yield criterion, and kinematic hardening rule is adopted in the analysis.

As for the concrete, compressive strength is assumed as 40 N/mm². In addition, tensile strength is assumed as one tenth of the compressive strength, as shown in Fig. 11 (c). Moreover, Young's modulus and Poisson's ratio are assumed as 30,500 N/mm² and 0.2, respectively. Non-linear behavior of the confined concrete is simulated by implementing the Mohr Coulomb yield criterion combined with the isotropic

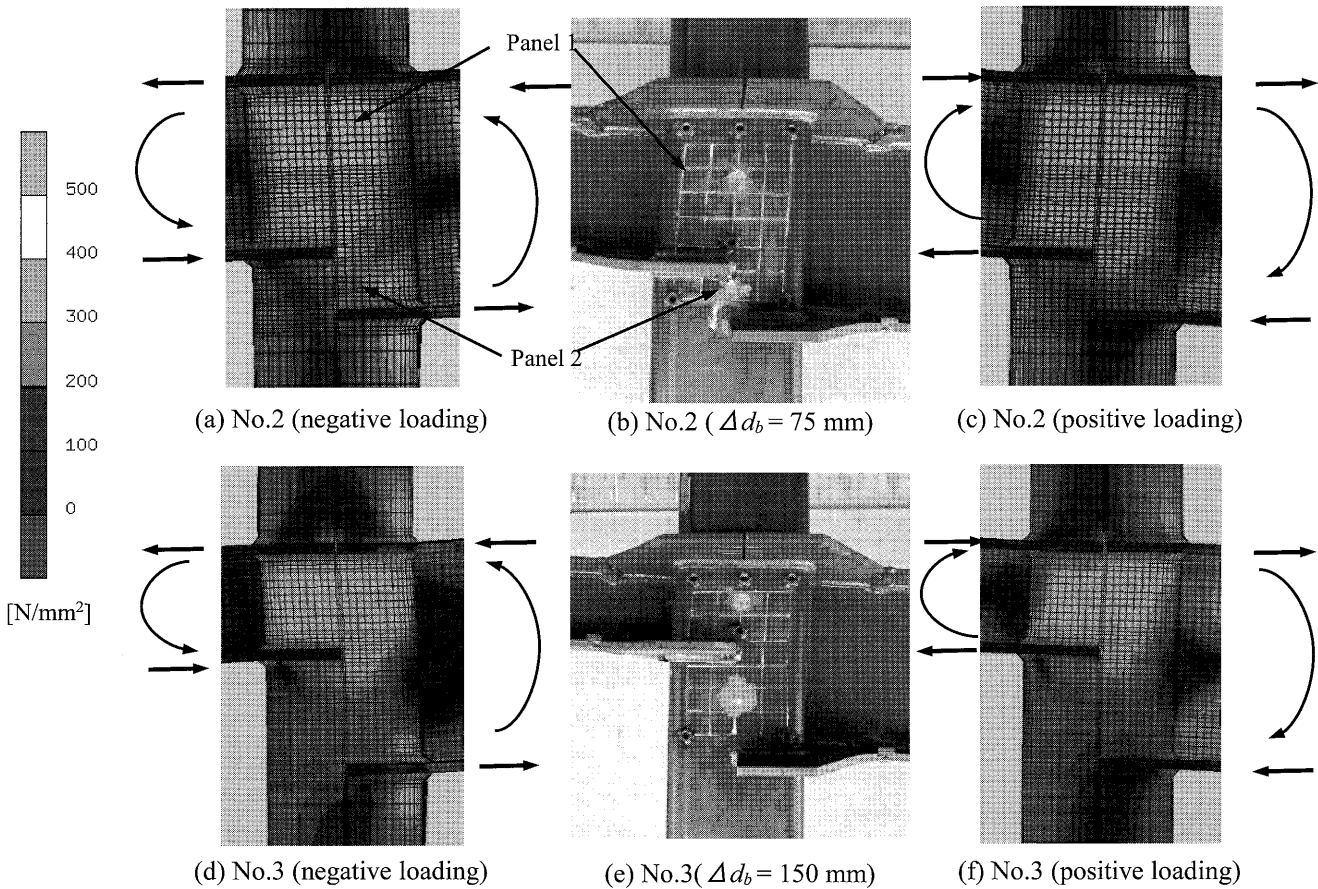


Fig. 9 Residual deformation of connection panel zone

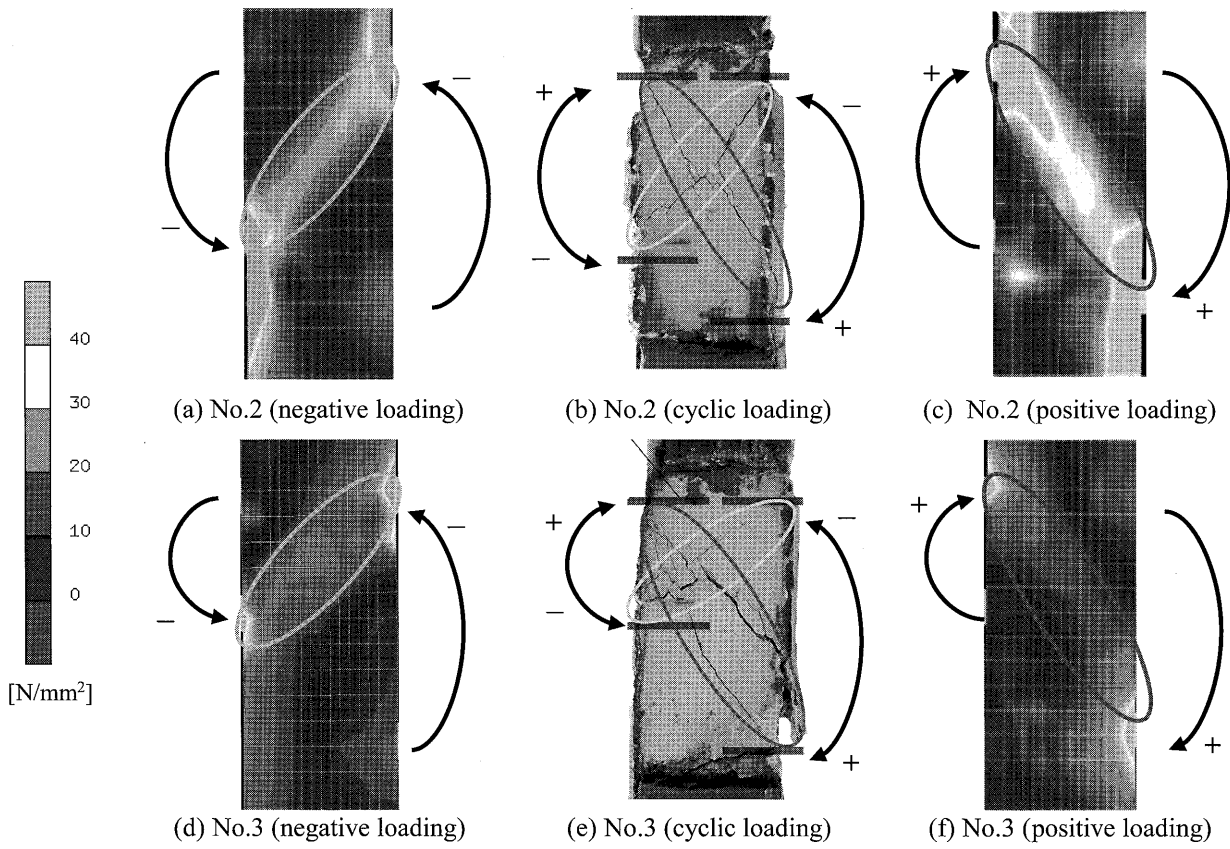


Fig. 10 Typical failure modes of core concrete

Table 5 Summary of offset beam-to-CFT column connection models

No.	Column (BCR295) [mm]	Beam1 (SN490B) [mm]	Beam2 (SN490B) [mm]	Δd_b [mm]
5	□-400×19	H-600×250×12×22	H-300×250×12×22	300
6	□-400×16	H-600×250×12×22	H-600×250×12×22	0
7	□-400×16	H-600×250×12×22	H-500×250×12×22	100
8	□-400×16	H-600×250×12×22	H-400×250×12×22	200
9	□-400×16	H-600×250×12×22	H-300×250×12×22	300
10	□-400×12	H-600×250×12×22	H-300×250×12×22	0
11	□-400×12	H-600×250×12×22	H-300×250×12×22	100
12	□-400×12	H-600×250×12×22	H-300×250×12×22	200
13	□-400×12	H-600×250×12×22	H-300×250×12×22	300
14	□-400×9	H-600×250×12×22	H-300×250×12×22	300

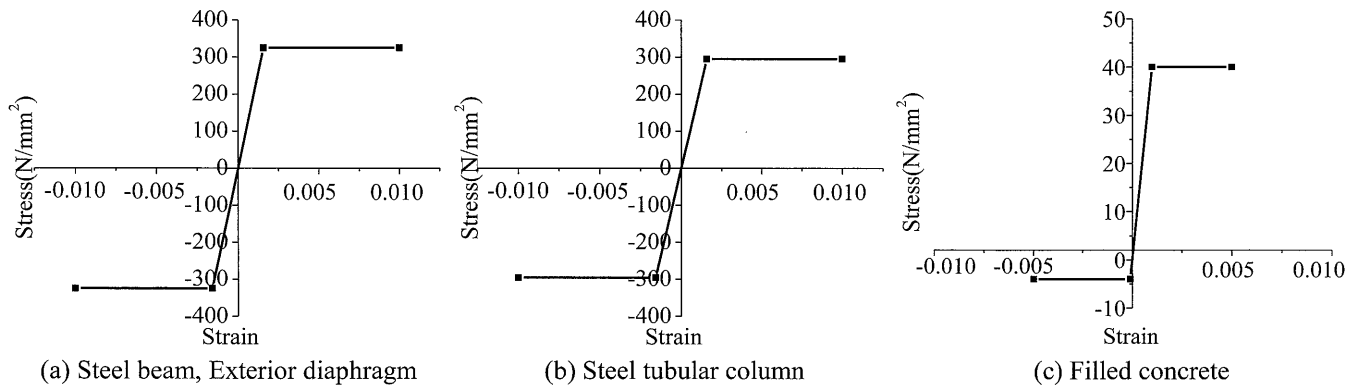


Fig. 11 Stress-strain relationship of steel and concrete

Table 6 Stiffness, yield shear strength and full plastic shear strength of entire panel

No.	D/t	Δd_b	Positive loading			Negative loading		
		mm	K [kN/rad]	pQ_{yFEM} [kN]	pQ_{pFEM} [kN]	K [kN/rad]	pQ_{yFEM} [kN]	pQ_{pFEM} [kN]
5	21	300	1,474,000	3141	3695	1,427,000	3171	3731
6	25	0	1,212,000	3433	3814	1,212,000	3433	3814
7	25	100	1,215,000	3164	3596	1,217,000	3246	3689
8	25	200	1,205,000	2927	3403	1,211,000	3030	3523
9	25	300	1,204,000	2701	3178	1,213,000	2724	3205
10	33	0	1,017,000	2944	3271	1,017,000	2944	3271
11	33	100	1,034,000	2645	3006	1,028,000	2749	3124
12	33	200	1,008,000	2475	2878	1,005,000	2577	2997
13	33	300	1,015,000	2321	2731	1,000,000	2382	2802
14	44	300	838,000	1943	2287	848,000	2024	2381

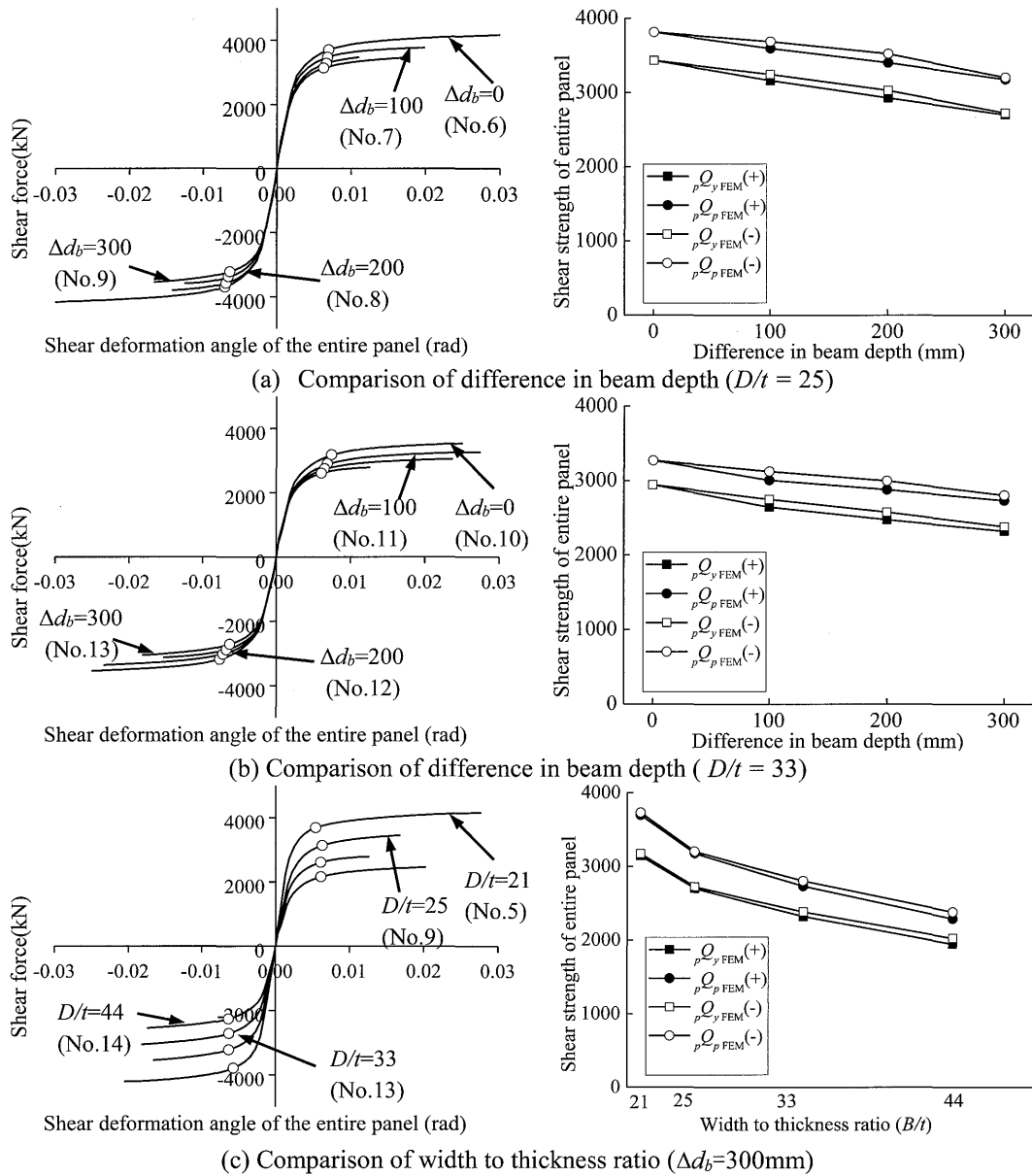


Fig. 12 Relation between shear force and shear deformation angle of entire panel

hardening rule. Softening modulus is assumed as 0.

Shear stiffness (K_{FEM}), yield shear strength (${}_pQ_{yFEM}$) and full plastic shear strength (${}_pQ_{pFEM}$) of the entire panel are summarized in Table 6. K_{FEM} is obtained by the secant modulus of shear force-shear deformation angle relationship from the original point to the point of $R = 0.005$ radian. Slope factor method is adopted to gain yield strength of connection panels⁸⁾. Relations between shear force and shear deformation angle of entire panel are shown in Fig. 12. The open circle represents the shear force of entire panel, when it reaches 0.35% offset strength point.

As the width to thickness ratio keeps constant (Figs. 12 (a) and (b)), with the increase of difference in beam depth, the yield strength and full plastic strength of the entire panel decrease. This indicates that the difference in beam depth has major impact on the yield strength and full plastic strength of entire panels. As the difference in beam depth keeps constant (Fig. 12 (c)), the yield shear strength and full plastic shear strength increase with the decrease of width to thickness ratio. This indicates that the width to thickness ratio has major impacts on the yield shear strength and full plastic shear strength of entire panels.

3. Collapse mechanisms and plastic strength

3.1 Collapse mechanism

In the companion paper, three types of collapse mechanisms were proposed¹⁾, as shown in Figs. 13 (a) to (f). The colored parts represent the yield fields of offset

beam-to-column connection when the entire panel zone gets into the plastic stage. Mechanism P_B matches well with the FEM results under negative loadings. However, mechanism P_A can't match well with the FEM results under positive loadings. Although the beam web affects the shear strength of entire panel, the contribution is very small. Therefore, the effect of the beam web on the shear strength of entire panel can be ignored.

The new collapse mechanism of steel parts under the positive loadings is shown in Fig. 14. The plastic deformation emerges on panel 1, out-of-plane deformation arises in the column flange connected with the exterior diaphragms.

3.2 Formulae of the plastic strength

(1) Contribution of steel parts

For the mechanisms E, P_B and new mechanism P_A, the internal virtual works of steel tube (${}_sW_p^E$, ${}_sW_p^{P_A}$ and ${}_sW_p^{P_B}$) are given by Eqs.(1) and (2)⁶⁾, respectively.

$${}_sW_p^E = 2td_c d_{b1} \frac{\sigma_{cy}}{\sqrt{3}} \Delta\theta \quad (1)$$

$${}_sW_p^{P_A} = {}_sW_p^{P_B} = 2td_c d_{b2} \frac{\sigma_{cy}}{\sqrt{3}} \Delta\theta \quad (2)$$

where, $d_c = D - t$; D : column width; t : column thickness; d_{b1} : distance between the centers of thickness of upper and lower flanges of beam 1; d_{b2} : distance between the centers of thickness of upper and lower flanges of beam 2; σ_{cy} : yield stress of steel tube; $\Delta\theta$: virtual rotational angle.

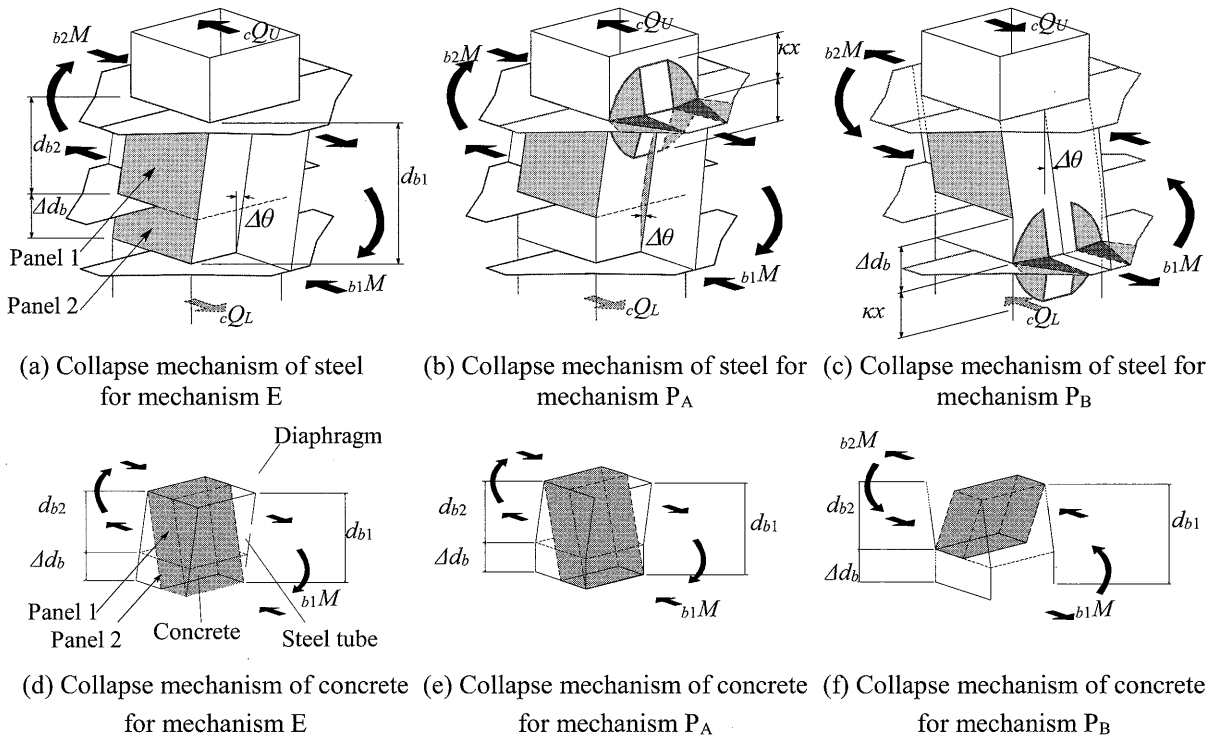


Fig. 13 Assumed collapse mechanism¹⁾

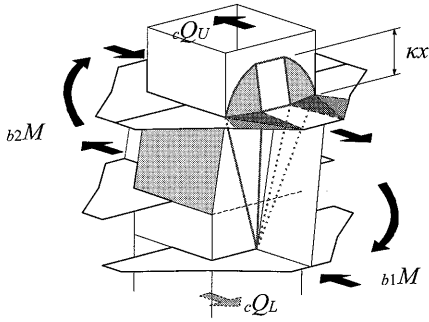


Fig. 14 Assumed collapse mechanism of steel parts for new mechanism P_A

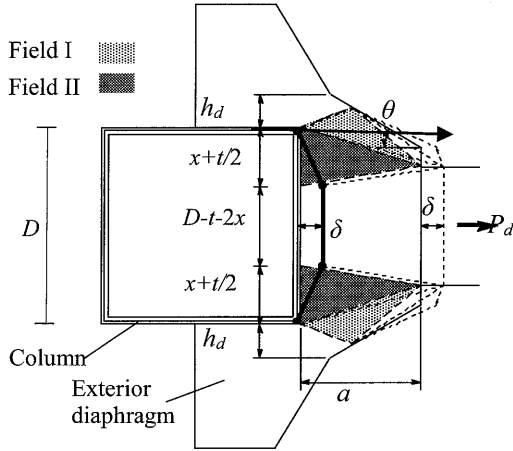


Fig. 15 Collapse mechanism of exterior diaphragm

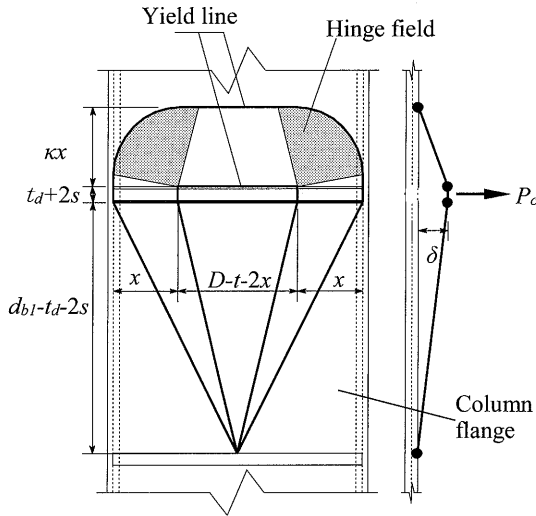


Fig. 16 Out of plane collapse mechanism of steel tubular wall for mechanism P_A

For the mechanisms P_A and P_B , the collapse mechanism of exterior diaphragm is shown in Fig. 15. The internal virtual work of exterior diaphragm (W_d) is given by Eq. (3)⁹.

$$W_d = \frac{\sqrt{3}}{3} t_d \cdot \sigma_{dy} \sqrt{4(x+t/2-b)^2 + a^2} \cdot \delta + \frac{2(1+\tan\theta)}{\sqrt{3(1+4\tan^2\theta)}} \cdot h_d t_d \sigma_{dy} \delta \quad (3)$$

where, x : plastic field parameter of the column flange; t_d : exterior diaphragm thickness; a : distance from the column face to the end of the exterior diaphragm; b : vertical distance from the corner of steel tube to the edge of beam flange; h_d : exterior diaphragm depth; σ_{dy} : yield stress of exterior diaphragm; θ : horizontal haunch angle; δ : virtual displacement of steel tube ($\delta = \Delta d_b \times \Delta\theta$).

For the mechanism P_A , the out-of-plane deformation of steel tubular flange is shown in Fig. 16. The internal virtual works of steel tubular flange (${}_sW_c^{P_A}$ and ${}_sW_c^{P_B}$) are given by Eqs. (4) and (5)¹.

$${}_sW_c^{P_A} = \left\{ \frac{\pi}{2} + \frac{2}{\pi} (\log_e \kappa)^2 + \frac{t_d + 2s}{x} + \frac{d_c}{2\kappa x} - \frac{1}{\kappa} + \frac{d_c - x}{2(d_{b1} - t_d - s)} + \frac{(d_{b1} - t_d - s)^2 + (d_c/2)^2}{2x(d_{b1} - t_d - s)} + \frac{(d_{b1} - t_d - s)^2 + (d_c/2 - x)^2}{2(d_c/2 - x)(d_{b1} - t_d - s)} \right\} \cdot t^2 \sigma_{cy} \delta \quad (4)$$

$${}_sW_c^{P_B} = \left\{ \frac{D-t-2x}{4} + \frac{D-t-2x}{2\kappa x} + \frac{t_d+2s}{x} + \frac{1}{\pi} \log_e \frac{\Delta d_b}{\pi} + \pi + \frac{2}{\pi} (\log_e \kappa)^2 + \frac{2}{\pi} (\log_e \frac{\Delta d_b}{\pi})^2 \right\} t^2 \sigma_{cy} \delta \quad (5)$$

where, s : weld size; κ : plastic field parameter of the column flange; Δd_b : difference in the beam depth.

Based on the virtual work principle, the external virtual work equals to the internal virtual work. Thus,

$${}_{ps}M_p^E \cdot \Delta\theta = {}_sW_p^E \quad (\text{for mechanism E}) \quad (6)$$

$${}_{ps}M_p^{P_A} \cdot \Delta\theta = {}_sW_p^{P_A} + {}_sW_c^{P_A} + W_d \quad (\text{for mechanism } P_A) \quad (7)$$

$${}_{ps}M_p^{P_B} \cdot \Delta\theta = {}_sW_p^{P_B} + {}_sW_c^{P_B} + W_d \quad (\text{for mechanism } P_B) \quad (8)$$

The full plastic moment of mechanism P_A and P_B (${}_pM_p^{P_A}$ and ${}_pM_p^{P_B}$) are given by Eqs. (9) and (10).

$${}_{ps}M_p^{P_A} = {}_pM_p^{P_A} - \frac{(cQ_U + cQ_L)}{2} \cdot \Delta d_b \quad (9)$$

$${}_{ps}M_p^{P_B} = {}_pM_p^{P_B} - \frac{(cQ_U + cQ_L)}{2} \cdot \Delta d_b \quad (10)$$

Based on upper bound theory, the parameters of x and κ are given by partial derivative.

$$\frac{\partial {}_{ps}M_p^{P_A}}{\partial \kappa} = 0, \quad \frac{\partial {}_{ps}M_p^{P_A}}{\partial x} = 0 \quad (11), (12)$$

$$\frac{\partial {}_{ps}M_p^{P_B}}{\partial \kappa} = 0, \quad \frac{\partial {}_{ps}M_p^{P_B}}{\partial x} = 0 \quad (13), (14)$$

For the positive loading, the minimum value between ${}_{ps}M_p^{P_A}$ and ${}_{ps}M_p^E$ is selected as the full plastic moment of the steel parts. While for the negative loading, the minimum

value between ${}_{ps}M_p^{P_B}$ and ${}_{ps}M_p^E$ is selected as the full plastic moment of the steel parts.

$${}_{ps}M_p^+ = \min\{{}_{ps}M_p^E, {}_{ps}M_p^{P_A}\} \quad (\text{under positive loadings}) \quad (15)$$

$${}_{ps}M_p^- = \min\{{}_{ps}M_p^E, {}_{ps}M_p^{P_B}\} \quad (\text{under negative loadings}) \quad (16)$$

The full plastic shear strengths of steel parts (${}_{ps}Q_p^E$, ${}_{ps}Q_p^{P_A}$ and ${}_{ps}Q_p^{P_B}$) are obtained by Eqs. (17) to (19).

$${}_{ps}Q_p^E = \frac{{}_{ps}M_p^E}{d_{b1}} \quad (\text{for mechanism E}) \quad (17)$$

$${}_{ps}Q_p^{P_A} = \frac{{}_{ps}M_p^{P_A}}{d_{b1}} \quad (\text{for mechanism } P_A) \quad (18)$$

$${}_{ps}Q_p^{P_B} = \frac{{}_{ps}M_p^{P_B}}{d_{b1}} \quad (\text{for mechanism } P_B) \quad (19)$$

(2) Contribution of concrete parts

The collapse mechanism of concrete panel is assumed as arch mechanism as shown in Fig. 17. The shear strength of concrete panel (${}_{pc}Q_p^E$, ${}_{pc}Q_p^{P_A}$ and ${}_{pc}Q_p^{P_B}$) are given by Eqs.(20) and (21) ²⁾.

$${}_{pc}Q_p^E = {}_{pc}Q_p^{P_A} = \frac{cD^2}{2} \left\{ \sqrt{1 + \left(\frac{d_{b1}}{cD}\right)^2} - \frac{d_{b1}}{cD} \right\} c\sigma_B \quad (20)$$

$${}_{pc}Q_p^{P_B} = \frac{cD^2}{2} \left\{ \sqrt{1 + \left(\frac{d_{b2}}{cD}\right)^2} - \frac{d_{b2}}{cD} \right\} c\sigma_B \cdot \frac{d_{b2}}{d_{b1}} \quad (21)$$

where, cD : core concrete width; $c\sigma_B$: concrete compressive strength.

Therefore, the full plastic shear strength of entire panel for mechanism E, mechanism P_A and mechanism P_B are obtained by Eqs.(22) to (24).

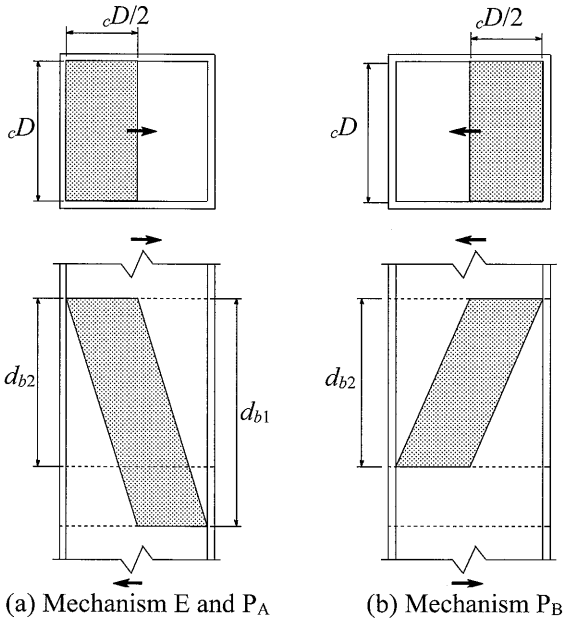


Fig. 17 Compression strut model of mechanism E, mechanism P_A and mechanism P_B

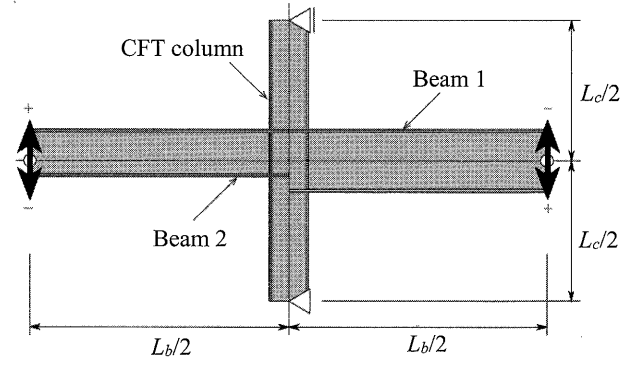


Fig. 18 Analysis model of parametric study

Table 7 Analysis conditions

Parameter	Value	Parameter	Value
D/t	20 to 45	D/t_d	20, 30
B_f/D	0.4, 0.6, 0.8	B_f/D_{b1}	0.5, 0.75
h_d/D	0.1, 0.2, 0.3	D_{b1}/L_c	0.15
$\Delta d_b/D_{b1}$	0.25, 0.5, 0.75	D/L_c	0.15
σ_B [N/mm ²]	30, 40, 50, 60		

B_f : Width of beam flange; Yield strength of steel tube: $\sigma_{cy}=295$ N/mm²; yield strength of beam and exterior diaphragm: $\sigma_{by}=\sigma_{dy}=325$ N/mm²;

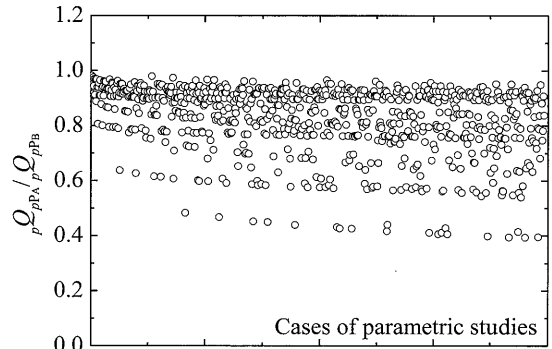


Fig. 19 Comparison between mechanism P_A and mechanism P_B

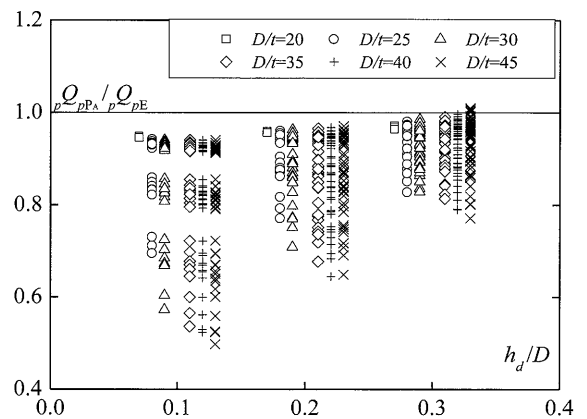


Fig. 20 Effects of size of exterior diaphragm

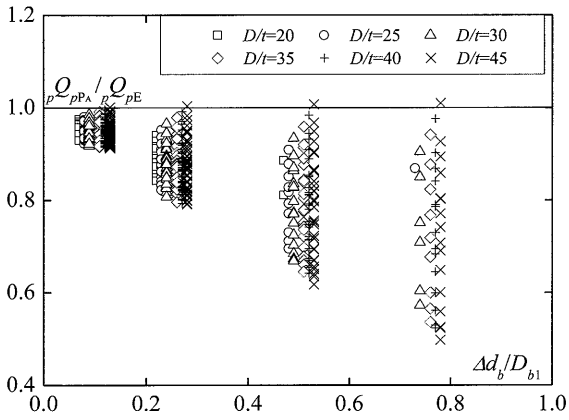


Fig. 21 Effects of difference in beam depth

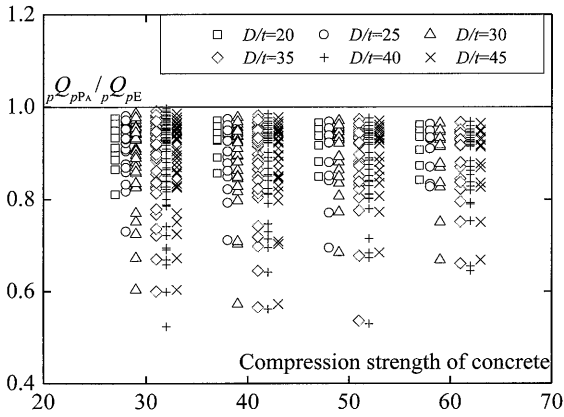


Fig. 22 Effects of compressive strength of concrete

$$pQ_p^E = p_s Q_p^E + p_c Q_p^E \quad (22)$$

$$pQ_p^{P_A} = p_s Q_p^{P_A} + p_c Q_p^{P_A} \quad (23)$$

$$pQ_p^{P_B} = p_s Q_p^{P_B} + p_c Q_p^{P_B} \quad (24)$$

3.3 Effects of parameters on the full plastic shear strength of offset beam-to-CFT column connection panel with exterior diaphragms

In this section, in accordance with the practical size of beam-to-CFT column connection with exterior diaphragms, the effects of parameters on the full plastic shear strength of offset panels are investigated. The analysis model of the offset-beam-to-CFT column connection with exterior diaphragms is shown in Fig. 18. And analysis conditions are listed in Table 7. Supposing the square steel tubular width is 400mm. The main parameters are width to thickness ratio of steel tube (D/t), size of exterior diaphragm, difference in beam depth and compressive strength of concrete.

Comparison between the full plastic shear strength obtained by mechanism P_A and mechanism P_B are shown in Fig. 19. With the change of parameters, pQ_{pPA} / pQ_{pPB} is less than 1.0. Based on the results of parametric and FEM studies, it is clear that full plastic strength of the entire panel under the negative loadings is a little larger than that under the positive

loadings. This means that owing to the influence of difference in beam depth, offset beam-to-column connection under the negative loadings is safer than that under the positive loadings. When offset beam-to-column connections are suffered from large earthquake, the offset beam-to-column connections are weaker and can damage firstly under the positive loadings, compared with those under the negative loadings. According to the capability of shear resistance, the shear strength obtained by mechanism P_B is larger than that obtained by mechanism P_A . Therefore, we only consider the minimum shear force (mechanism P_A) and ignore the shear force obtained by mechanism P_B in the design.

Figs. 20 to 22 show the effects of size of exterior diaphragm, difference in beam depth and compressive strength of concrete on the full shear strength of the offset panel. As for Fig. 20, it is found that with the increases of size of exterior diaphragm, pQ_{pPA} / pQ_{pPE} increases. One reason is that with the size of exterior diaphragm increases, the contribution of exterior diaphragm on the full plastic shear strength of offset panel becomes large.

As for width to thickness ratio ranging from 15 to 40, shown in Fig. 21, with the difference in beam depth increases, the pQ_{pPA} / pQ_{pPE} decreases. One reason is that with the difference in beam depth increases, the contribution of steel panel on the full shear strength of the offset panel becomes small. Therefore, the full plastic shear strength of steel panel 1 obtained by mechanism P_A decreases. As for D/t equal to 45 and 50, with the difference in beam depth increases, the upper limit of pQ_{pPA} / pQ_{pPE} increases. One reason is that with large D/t , the contribution of steel panel on the full shear strength of the offset panel becomes small obtained by mechanism E.

As for Fig. 22, with the changes of compressive strength of concrete, there is no significant difference in the pQ_{pPA} / pQ_{pPE} . This is because with the increases of compressive strength of concrete, both the full plastic strength obtained by mechanism E and that obtained by mechanism P_A increases.

According to FEM results and parametric studies, the full plastic strength of the entire panel under the negative loadings is a little larger than that under the positive loadings. Therefore, the full plastic shear strength of the entire panel under the negative loadings need not be considered. The shear forces of entire panel obtained by calculation formulae are listed in Table 9. Comparing the residual deformation of specimens with the assumed collapse mechanisms, the failure modes of No.2 and No.3 match well with the mechanism P_A . Therefore, the calculated shear strengths of No.2 and No.3 follow mechanism P_A .

The comparisons among the strength calculation results (pQ_{pc}), the experimental strength results (pQ_{pe}) and FEM strength results (pQ_{pFEM}) for the entire panel are listed in Table 10. The plastic strength (pQ_{pg}) is suggested by the CFT recommendation, which is obtained by Fukumoto model ¹⁾.

The calculated results of No.2 and No.3 are smaller than that of No.1. Meanwhile, with the difference in beam depth increase, the calculated value decrease. This is consistent with the tendency of the experimental and FEM results.

Comparing the calculated results with the experimental and FEM results, the calculation results underestimate the

Table 9 Calculated shear strength of entire panel

No.	Δd_b (mm)	pQ_p^E (kN)	pQ_p^{PA} (kN)
1	0	992	-
2	75	995	930
3	150	1,001	876

Table 10 Comparisons among the experimental, analytical and calculated results

No.	Δd_b (mm)	pQ_{pc} (kN)	pQ_{pe} (kN)	pQ_{pFEM} (kN)	$\frac{pQ_{pc}}{pQ_{pe}}$	$\frac{pQ_{pc}}{pQ_{pFEM}}$	pQ_{pg} (kN)
1	0	992	1,119	1,094	0.88	0.90	1,109
2	75	930	1,033	1,004	0.90	0.92	-
3	150	876	918	897	0.95	0.97	-

Where, pQ_{pc} : shear force of entire panel obtained by calculation formulae; pQ_{pe} : 0.35% offset shear strength of entire panel obtained by experimental results; pQ_{pFEM} : 0.35% offset shear strength of entire panel obtained by FEM results; pQ_{pg} : shear force of entire panel obtained by Fukumoto formulae ²⁾.

Table 11 Comparisons between formulae and analytical shear force for analytical models

No.	Column	Δd_b mm	pQ_{pFEM} (kN)	pQ_p^E (kN)	pQ_p^{PA} (kN)	$\frac{pQ_{pc}}{pQ_{pFEM}}$
5	□-400×19	300	3,695	3,218	2,907	0.78
6	□-400×16	0	3,814	2,882	-	0.76
7	□-400×16	100	3,596	2,882	2,812	0.77
8	□-400×16	200	3,403	2,882	2,748	0.80
9	□-400×16	300	3,178	2,882	2,637	0.82
10	□-400×12	0	3,271	2,424	-	0.74
11	□-400×12	100	3,006	2,424	2,419	0.79
12	□-400×12	200	2,878	2,424	2,412	0.83
13	□-400×12	300	2,731	2,424	2,408	0.87
14	□-400×9	300	2,287	2,076	2,078	0.90

Table 12 Enhancement coefficient obtained from test results

No.	$p_s Q_p$ (kN)	$p_c Q_p$ (kN)	$p Q_{pe}$ (kN)	$p_s Q_p - p Q_{pe}$ (kN)	k_e	$p Q_{pFEM}$ (kN)	$p Q_{pFEM} - p_s Q_p$ (kN)	k_{FEM}
1	820	172	1,119	299	1.74	1,094	274	1.59
2	755	175	1,033	278	1.59	1,004	244	1.42
3	700	176	918	218	1.24	897	197	1.20

Table 13 Enhancement coefficient obtained from FEM analysis results

No.	$p_s Q_p$ (kN)	$p_c Q_p$ (kN)	$p Q_{pFEM}$ (kN)	$p Q_{pFEM} - p_s Q_p$ (kN)	k_{FEM}
5	2,203	753	3,695	1,492	1.98
6	2,093	789	3,814	1,721	2.18
7	2,031	789	3,596	1,565	1.98
8	1,975	789	3,403	1,428	1.81
9	1,923	789	3,178	1,255	1.59
10	1,585	839	3,271	1,686	2.01
11	1,582	839	3,006	1,424	1.70
12	1,579	839	2,878	1,299	1.55
13	1,576	839	2,731	1,155	1.38
14	1,199	877	2,287	1,088	1.24

experimental and analytical results. While, the full plastic shear strength of entire panel for No.1 proposed by Fukumoto model matches well with the experimental and analytical results. One of the reason is that the Fukumoto model takes the confined effect provided by the steel tubular flange into account.

The full plastic shear strength of the entire panel obtained from the proposed formulae are compared with those obtained by FEM results in Table 11. The full plastic strengths by the proposed formulae are between 74% - 90% of analytical results. Comparing the formulae results with the analytical results, the mean ratio of the formulae results to the analytical results is 0.804 for all 10 models, and the standard deviation and the corresponding coefficient of variation are 0.027 and 0.033, respectively.

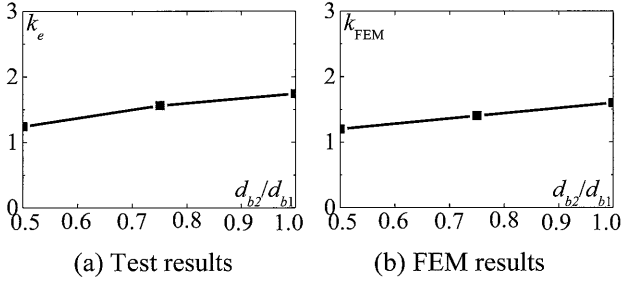
4. Confined effect on concrete

4.1 Enhancement coefficient

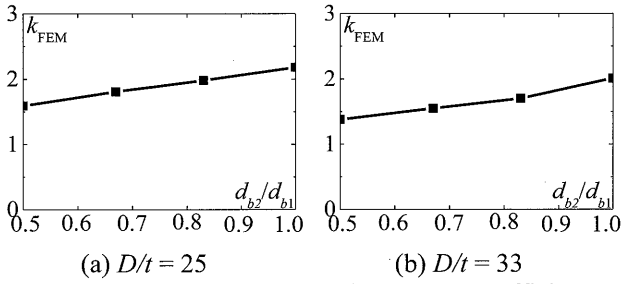
In the previous section, owing to overlooking the confined effect on concrete, the proposed formulae underestimated the shear strength of the offset panel. Therefore, the shear capability enhancement coefficient for the full plastic strength is assumed to be defined as Eq.(25).

$$k = \frac{p Q_p - p_s Q_p}{p_c Q_p} \quad (25)$$

where, pQ_p : experimental strength of the offset panel; psQ_p : shear strength of the steel parts, which is obtained by Eq.(17) or (18); pcQ_p : shear strength of the concrete panel obtained by Eq.(20).



(a) Test results (b) FEM results
Fig. 23 Relation between enhancement coefficient and difference in beam depth



(a) $D/t = 25$ (b) $D/t = 33$
Fig. 24 Relation between the enhancement coefficient and beam depth ratio

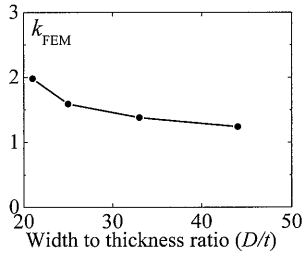
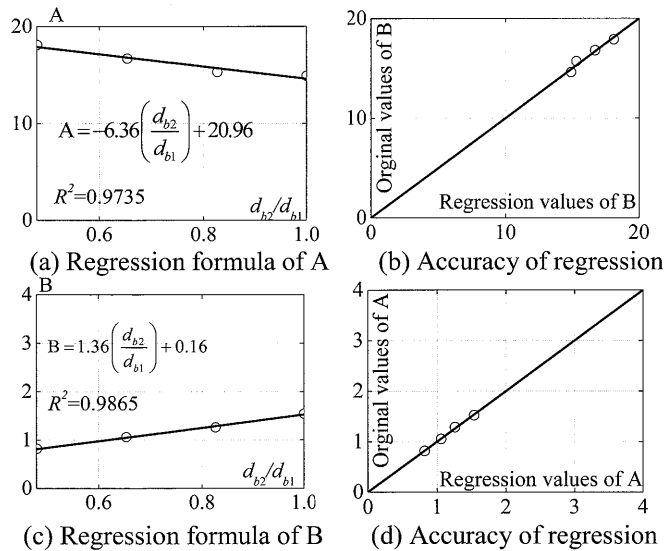


Fig. 25 Relation between the enhancement coefficient and width to thickness ratio



(a) Regression formula of A (b) Accuracy of regression
(c) Regression formula of B (d) Accuracy of regression
Fig. 26 Regression analysis and accuracy of regression analysis result

Table 12 lists the enhancement coefficients obtained by Eq.(25). Relations between enhancement coefficient and beam2 depth to beam1 depth ratio (hereinafter beam depth ratio) are shown in Fig. 23. It is obvious that with the beam depth ratio increases, the enhancement coefficient increases. Therefore, the enhancement coefficients should take the effect of beam depth ratio into consideration.

The enhancement coefficients of the offset beam-to-CFT column connection panels for other ten analytical models are summarized in Table 13. Relations between the enhancement coefficient and beam depth ratio are shown in Fig. 24. As the width to thickness ratio keeps constant, the enhancement coefficient increases with the increase of beam depth ratio. This also indicates that the beam depth ratio has influence on the enhancement coefficients.

Relation between the enhancement coefficient and width to thickness ratio is shown in Fig. 25. As the difference in beam depth keeps constant ($\Delta d_b = 300\text{mm}$), the enhancement coefficient decrease with the width to thickness ratio increases. It indicates that the width to thickness ratio affects the enhancement coefficient.

4.2 Regression analysis

Multivariable regression analyses are conducted in order to propose a formula for calculating the enhancement coefficient. According to the previous researches on beam-to-square CFT column connection with exterior diaphragms²⁾, the width to thickness ratio of beam-to-CFT column connection with exterior diaphragms ranges from 23.3 to 64.8. According to the previous researches on offset beam-to-column connection^{6,9)}, beam depth ratio ranges from 0.45 to 1.0.

The analytical ranges of beam depth ratio (d_{b2}/d_{b1}) and width to thickness ratio (D/t) of steel tube adopted in the analysis of this study are generally cover the ranges of the above. In the following regression analysis, the ranges of d_{b2}/d_{b1} and D/t are assumed to be from 0.48 to 1.0 and from 22 to 45, respectively.

Supposing k and $(D/t-2)^{-1}$ ($0.02 < (D/t-2)^{-1} < 0.055$) are linear correlation, the linear regression equation is determined by Eq.(26).

$$k = A \cdot (D/t-2)^{-1} + B \quad (26)$$

where, B and A are obtained by Eqs.(27) and (28).

$$A = \frac{\sum_{i=1}^n (D/t-2)^{-1}_i \cdot k_{FEMi} - n \cdot \overline{(D/t-2)^{-1}} \cdot \overline{k_{FEM}}}{\sum_{i=1}^n (D/t-2)^{-2}_i - n \cdot \left(\overline{(D/t-2)^{-1}}\right)^2} \quad (27)$$

$$B = \overline{k_{FEM}} - A \cdot \overline{(D/t-2)^{-1}} \quad (28)$$

where, i : number of FEM models; $\overline{k_{FEM}}$: arithmetic mean of k_{FEM} ; $\overline{(D/t-2)^{-1}}$: arithmetic mean of $(D/t-2)^{-1}$.

The value k is proposed by Eqs.(29) to (32).

$$k_1 = 18.1t / (D - 2t) + 0.82 \quad (d_{b2}/d_{b1} = 0.48) \quad (29)$$

$$k_2 = 16.7t / (D - 2t) + 1.06 \quad (d_{b2}/d_{b1} = 0.65) \quad (30)$$

$$k_3 = 15.3t / (D - 2t) + 1.26 \quad (d_{b2}/d_{b1} = 0.82) \quad (31)$$

$$k_4 = 14.9t / (D - 2t) + 1.54 \quad (d_{b2}/d_{b1} = 1.00) \quad (32)$$

Owing to the influence of difference in beam depth, the regression formulae are different. Supposing there are linear correlation between A and d_{b2}/d_{b1} or B and d_{b2}/d_{b1} . The regression formula and its accuracy are shown in Fig.26. As shown in Fig. 26, the values B and A are proposed by Eqs.(33) and (34).

$$A = -6.36(d_{b2} / d_{b1}) + 20.96 \quad (33)$$

$$B = 1.36(d_{b2} / d_{b1}) + 0.16 \quad (34)$$

Based on the regression analysis, the enhancement coefficient is given by Eq.(35).

$$k = \left(-6.36 \cdot \frac{d_{b2}}{d_{b1}} + 20.96 \right) \cdot \left(\frac{D}{t} - 2 \right)^{-1} + 1.36 \left(\frac{d_{b2}}{d_{b1}} \right) + 0.16 \quad (35)$$

where, D : column width; t : column thickness; d_{b1} : distance between the centers of thickness of upper and lower flanges of beam 1; d_{b2} : distance between the centers of thickness of upper and lower flanges of beam 2.

The comparisons between the enhancement coefficients obtained by FEM results (k_{FEM}) and those calculated by formulae (k_F) are listed in Table 14.

As for the FEM models in column width of 400mm, the enhancement coefficients proposed by formulae are between 98% - 105% of analytical results. Comparing the formulae results to the analytical results, the mean ratio of the formulae results to the analytical results is 1.00 for all 10 models, and the standard deviation and the corresponding coefficient of variation are 0.023 and 0.023, respectively. As for all of the analytical models, the enhancement coefficient formulae results have high accuracy. The comparisons among k_{FEM} , k_e and k_F are illustrated in Fig. 27. It is obvious that for the 10 analytical models in column width of 400mm, the enhancement coefficients proposed by formulae have good agreements with those obtained by FEM results.

However, as for No.1 to No.3, the enhancement coefficients proposed by the formula are from 139% to 141% of analytical results and from 129% to 137% of experimental results. The proposed formula overestimates the enhancement coefficient obtained by experimental and FEM results. One reason is that the proposed formula doesn't take the effect of compressive strength of concrete and yield strength of steel tube into consideration.

4.3 Comparison between strength by FEM analysis and that by the proposed formulae

Considering the confined effect on the full plastic strength of entire panel, the proposed formulae Eqs.(22) and (23) are changed into Eqs.(36) and (37).

$${}_p Q_p^E = {}_{ps} Q_p^E + k_F \cdot {}_{pc} Q_p^E \quad (36)$$

$${}_p Q_p^{EA} = {}_{ps} Q_p^{EA} + k_F \cdot {}_{pc} Q_p^{EA} \quad (37)$$

The full plastic strength of the entire panel obtained from proposed formulae (${}_p Q_{pc}$) are compared with those by FEM analysis (${}_p Q_{pFEM}$) in Table 15. The full plastic strengths by the

Table 14 Comparisons between k_{FEM} and k_F

No.	k_{FEM}	k_F	$\frac{k_F}{k_{FEM}}$
1	1.59	2.24	1.41
2	1.42	1.97	1.39
3	1.20	1.70	1.41
5	1.98	1.95	0.98
6	2.18	2.15	0.99
7	1.98	1.97	0.99
8	1.81	1.78	0.98
9	1.59	1.59	1.00
10	2.01	1.99	0.99
11	1.7	1.79	1.05
12	1.55	1.59	1.02
13	1.38	1.39	1.00
14	1.24	1.24	1.00

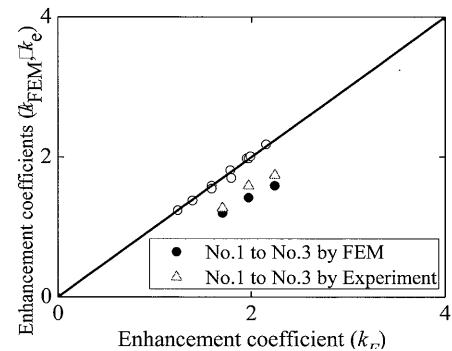


Fig. 27 Comparisons between k_{FEM} and k_F

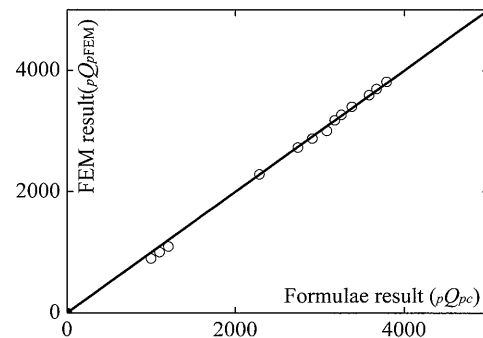


Fig. 28 Comparisons between formulae and FEM results

proposed formulae are between 98% - 116% of analytical results. The mean ratio of the formulae results to the analytical is 1.04 for all 13 models, and the standard deviation and the corresponding coefficient of variation are 0.027 and 0.025, respectively. Comparing the formulae results with the analytical results, the formulae results have good accuracy. The comparisons between pQ_{pFEM} and pQ_{pc} are illustrated in Fig. 28. It is obvious that for the 13 analytical models, the formulae results have good agreements with those obtained by FEM results.

Table 15 Comparison between formulae and FEM results

No.	pQ_{pFEM} (kN)	pQ_{pc} (kN)	$\frac{pQ_{pc}}{pQ_{pFEM}}$
1	1,094	1,207	1.10
2	1,004	1,123	1.10
3	897	1,042	1.11
5	3,695	3,637	0.99
6	3,814	3,757	0.99
7	3,596	3,609	1.00
8	3,403	3,466	0.99
9	3,178	3,252	1.00
10	3,271	3,212	0.99
11	3,006	3,040	1.03
12	2,878	2,957	1.01
13	2,731	2,861	1.00
14	2,287	2,394	1.00

5. Conclusive Remarks

This paper presents FEM analytical investigation on the offset beam-to-CFT column connection panels with exterior diaphragms and assumed the collapse mechanisms of the offset beam-to-CFT column connection panels. Based on the assumed collapse mechanisms, calculation formulae of the full plastic shear strength of the offset panels were proposed. On the basis of experimental and analytical results, an enhancement coefficient formula was proposed, which was derived from regression analysis taking the effect of width to thickness ratio of steel tubes and beam depth ratio into consideration. Some achievements have been obtained as follows:

- (1) Based on the experimental and analytical results, the collapse mechanisms of the offset panels were proposed. These mechanisms are considered to explain the collapse characteristics of the offset beam-to-CFT column connection panels with exterior diaphragms.
- (2) The enhancement coefficient of the offset beam-to-CFT column connection panels could be evaluated by Eq.(35). As for the FEM models in column width of 400 mm, the enhancement coefficients calculated by the proposed formula had good agreements with those

obtained by FEM results. However, as for the three test specimens, the calculated enhancement coefficient overestimated the FEM results. One of the reasons was considered that the proposed formula didn't take the effect of compressive strength of concrete and yield strength of steel tube into consideration.

- (3) Comparing the full plastic strengths of the offset panel obtained from Eqs. (36) and (37) with those obtained by FEM analysis, the calculated results had good agreements with the FEM results.

Acknowledgements

A part of this study was financially supported by Grant-in-Aid for Scientific Research (B) No. 25820268. The computation was mainly carried out by computer facilities at Research Institute for Information Technology, Kyushu University.

REFERENCES

- 1) Recommendations for Design and Construction of Concrete Filled Steel Tubular Structures, Architectural Institute of Japan, AIJ, Japan, 2008.
- 2) B. Mou, S. Matsuo, R. Ikeda and A. Kawano: An Experimental Study on Offset H-shaped Steel Beams to Square Concrete Filled Steel Tubular Column Connection Panels with Exterior Diaphragms, Journal of Architecture and Urban Design, Kyushu University, No. 26, pp. 101-110, July, 2014.
- 3) Y. M. Alostaz and S. P. Schneider: Analytical Behaviour of Connections to Concrete-filled Steel Tubes, Journal of Constructional Steel Research, No. 40(2), pp. 95-127, 1996.
- 4) S. P. Chiew, S. T. Lie and C. W. Dai: Moment Resistance of Steel I-beam to CFT Column Connections, Journal of Structural Engineering, ASCE, No. 127 (10), pp.1164-1172, 2001.
- 5) MSC, Software Corporation, MSC. Marc User's Manual (Marc 2012, volume A, theory and user information) (2012) [Santa Ana, CA 92707, USA]
- 6) S. Kuwahara, T. Kumano and K. Inoue: The Elasto-Plastic Behavior of Joint Panels at the Connection of Rectangular Steel Column and Two H-shaped Beams with Different Depth, J. Struct. Constr., AIJ, No.533, pp. 175-181, July, 2000. (in Japanese)
- 7) International building code, International code council, INC, 2009.
- 8) L. S. Beedle, A. A. Topractsologlou and B. G. Johnston: Connection for Welded Continuous Portal Frames (part III Discussion of Test Results and Conclusions), Progress report NO.4, The Welding Journal, 543-s-560-s, Nov., 1952.
- 9) S. Matsuo, T. Tanaka and K. Inoue: Design Formulae for RHS-column to Beam Connections with Exterior Diaphragms, J. Struct. Constr., AIJ, No.618, pp. 221-228, Aug., 2007 (in Japanese)

(受理：平成27年6月11日)